Geophys. J. Int. (1990) **102,** 89–100

Modelling curved surface wave paths: membrane surface wave synthetics

T. Tanimoto
Seismological Laboratory, 252-21 California Institute of Technology, Pasadena, CA 91125, USA

Accepted 1990 January 3. Received 1990 January 2; in original form 1988 November 12

SUMMARY

Earth's heterogeneity near the surface is so severe that surface waves with period 20 s exhibit complicated propagation effects such as curved paths and multiple rays. In order to take account of these effects, a new method to analyse surface waves is developed. The method, which we call the membrane surface wave method, is an approximation to the Green's function method in a 3-D medium and is valid for a laterally, smoothly varying media. We also present the formulae to invert the seismograms. As an example, we apply the method to a preliminary California model. Use of the method for the forward calculation shows that heterogeneity in the model is so severe that the wavefront due to the Whittier Narrows earthquake is split in two by the time it reaches the San Francisco Bay area. The kernels in the inverse formula to the six Berkeley stations show curved paths, multipathings and finite wavelength effects and visually demonstrate how waves sample the medium. The method is attractive in that these complications cause no problems in its application.

Key words: inversion, seismograms, surface waves.

1 INTRODUCTION AND MOTIVATION

Recent global scale structure studies have used very long-period surface waves (longer than 100 s) to retrieve the upper mantle structure (e.g. Woodhouse & Dziewonski 1984; Tanimoto 1988). The basic reason behind this was that shorter period surface waves exhibit such strong effects of lateral heterogeneity that the economical perturbation approach (Woodhouse & Dziewonski 1984) from the laterally homogeneous medium does not work very well. Various methods such as coupling calculations (e.g. Park 1987; Tsuboi & Geller 1989), ray theoretical approaches (e.g. Woodhouse & Wong 1986) and Gaussian beam approaches (e.g. Yomogida 1985) have been tried with some success. Each method, however, has some disadvantages. For example, coupling calculations become computationally difficult in the short-period range (<40 s) where the density of modes is very high. Ray properties of waves such as arrival times have been remarkably useful even for long-period waves (phase and group velocity) and Woodhouse & Wong (1986) showed that it also works for amplitudes to a certain extent. But it is not so clear why ray theory can be used for long-period waves. Wavelengths of such waves are much larger than the scale of heterogeneity in many applications, which is a violation of one of the basic assumptions in ray theory. The Gaussian beam method is an interesting, economical approach but its arbitrariness in the choice of beam width deterred some researchers from its use.

In this paper, we present a new method to generate synthetic seismograms for a laterally heterogeneous medium. The method is based on the Green's function approach in a fully 3-D medium. Assumptions for surface waves in a laterally, smoothly varying medium allow the problem to be reduced to the 2-D problem. Since the problem amounts to solving a 2-D problem by a numerical method, we call it the membrane surface wave method. The form of the solution was first discussed by Dahlen (1980) and an application to great circle waves in a different context has been done by Dahlen & Henson (1985) and Henson & Dahlen (1986).

Our approach is similar to that of Sword, Claerbout & Sleep (1989), who applied the finite element method to a spherical global earth model. They have shown how the acoustic waves can be effectively simulated on a sphere. The example in this paper for a spherical case is similar to their calculation, because the potential for surface waves follow acoustic wave type equation under our assumptions. Technically, our approach is different; we use the finite difference method to a region bounded by constant latitudes and longitudes with absorbing boundary conditions.

We also present formulae for inversion. The kernels in

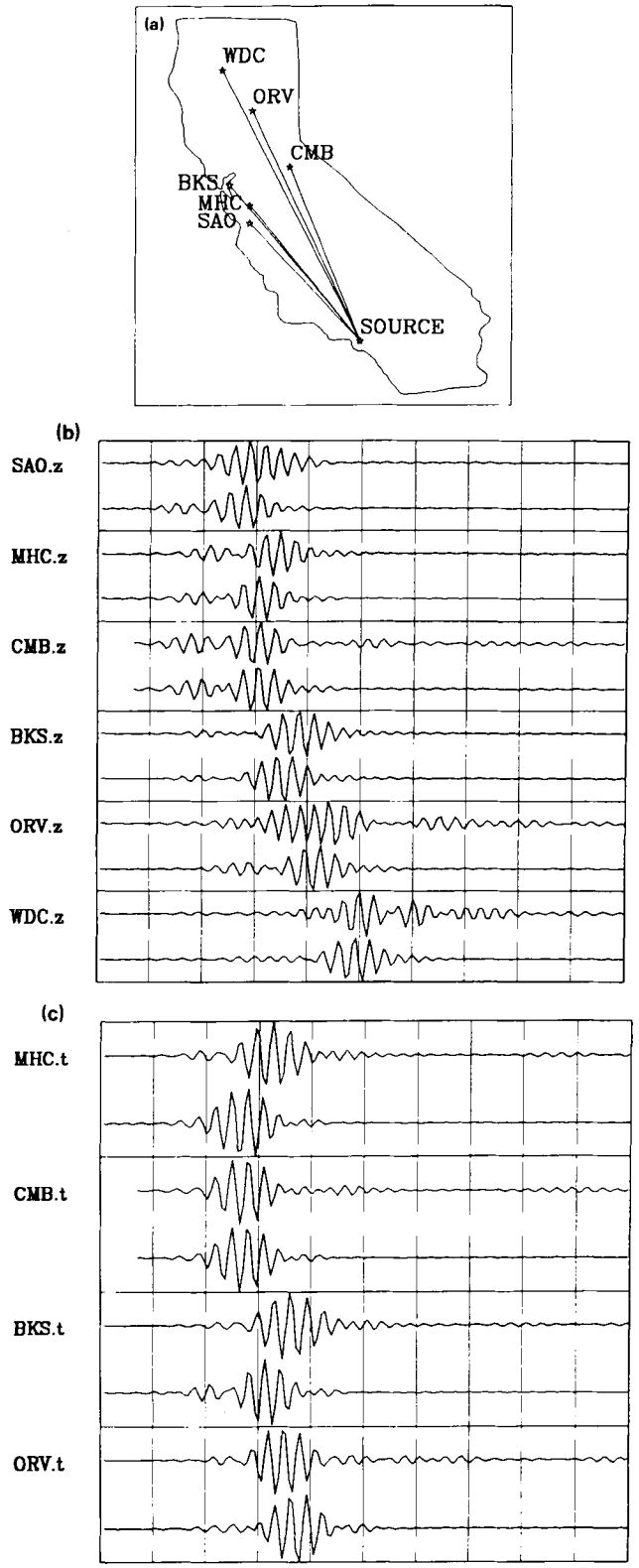

Figure 1. (a) Location of the source (the Whittier Narrows earthquake) and the six Berkeley stations. (b) Filtered Rayleigh wave (vertical component) data. For each data, a synthetic seismogram is shown below. Vertical lines are given at 1 min intervals. Note the difference in arrival time of wave packets at CMB and MHC, which are at almost the same epicentral distance. (c) Filtered Love wave data. Paths to CMB and ORV, which go through the Sierra Nevada are clearly fast.

the inverse formulae are especially useful in understanding what happens during the process of inversion. We show some examples in which kernels demonstrate curved paths and multipathings. It is a good way to understand complicated propagation effects intuitively. Tarantola (1984) derived an inversion algorithm which essentially avoids the computation of kernels for a 3-D problem. His method is quite ingenious and attractive, but we believe it is important to examine the kernels and understand the overall situation during the course of inversion.

In order to demonstrate the degree of heterogeneity in a continental, regional problem, we show the records of six Berkeley stations in Figs 1(a)–(c). These data were obtained from the Berkeley Digital Seismograph Network of the University of California. They were reported in Bolt, Lomax & Uhrammer (1989). Fig. 1(a) shows the locations of the earthquake, the Whittier Narrows earthquake of 1987 October 1, and the six Berkeley stations. Fig. 1(b) shows Rayleigh waves (vertical component) and Fig. 1(c) shows four Love wave records. Each record was filtered between 40 and 70 mHz, and a synthetic seismogram is given below each seismogram. Vertical lines are drawn at intervals of 1 min. Synthetic seismograms are calculated for a model suitable for Southern California (Hadley & Kanamori 1977) by the normal mode summation method.

One of the interesting results in these records appears in comparing the seismograms at CMB and MHC. The epicentral distances to the two stations are practically the same (487 km to MHC and 488 km to CMB), which can be confirmed from the similarity of synthetic seismograms. But the path to MHC is in the coastal range while the path to CMB is in the Sierra Nevada. Because of the structure difference between the two regions, the data show a huge difference in arrival times of approximately 25 s. This amounts to about 20 per cent of the traveltime and thus group and phase velocity for these paths differ by about 20 per cent. The assumption of wave propagation along straight paths clearly does not work in such a medium. The problem requires a method that takes into account complicated propagation effects; this is the basic motivation of developing the method we describe hereafter.

2 BASIC FORMULAE

The basic assumption in our approach is that Rayleigh wave displacement is given within a narrow frequency band by

$$\mathbf{u} = U(z)\mathbf{z}\phi_R + V(z)\nabla_1\phi_R \tag{2.1}$$

and Love wave displacement by

$$\mathbf{u} = W(z)(-\mathbf{z}\times\nabla_1)\phi_T. \tag{2.2}$$

In these formulae, $U(z)$, $V(z)$ and $W(z)$ are vertical eigenfunctions, ϕ_R and ϕ_T are potentials for Rayleigh and Love waves, $\mathbf{z}$ is the unit vector in the vertical direction and ∇_1 denotes surface differentiation, i.e. in Cartesian coordinates

$$\nabla_1 = \mathbf{x}\frac{\partial}{\partial x} + \mathbf{y}\frac{\partial}{\partial y}.$$

These formulae are valid only for a narrow frequency band since we assume that eigenfunctions remain unchanged as surface waves propagate.

The potentials ϕ_R and ϕ_T satisfy the equation

$$\nabla_1^2\phi + \frac{\omega^2}{c(x, y)^2}\phi = 0 \tag{2.3}$$

where the subscript R or T is dropped, and c is the Rayleigh or Love wave phase velocity, as required.

Another assumption required for (2.1) and (2.2) is that lateral variation of elastic constants (λ and μ) be smooth. Specifically, if we take $\partial_x[(\lambda+\mu)U\partial_x\phi]$ as an example, this is approximately

$$\frac{\partial}{\partial x}\left[(\lambda+\mu)U\frac{\partial\phi}{\partial x}\right] \approx (\lambda+\mu)U\frac{\partial^2\phi}{\partial x^2} \tag{2.4}$$

where we neglect terms containing derivatives of λ and μ with respect to x. This approximation means that lateral variation of elastic constants within a wavelength is small. In this respect, this theory is similar to ray theory and to free oscillation (surface wave) studies which assume $l \gg s$ where l is the angular degree of waves and s is the angular degree of heterogeneity.

Under these assumptions, we can verify the validity of (2.1), (2.2) and (2.3) by directly substituting (2.1) or (2.2) into the elastodynamic equations of motion. Since this is straigthforward, we give the details in the Appendix.

3 FORMULAE FOR INVERSION

We derive the formulae for the inversion in this section. The basic approach is the use of Green's functions and their reciprocity relations. We first derive expressions that are valid in 3-D structures and then substitute (2.1) or (2.2) to obtain the expressions for surface waves.

3.1 Formulae in the 3-D media

We denote the x, y and z components of displacement by u, v and w and their perturbation by δu, δv and δw. We also denote perturbation of elastic constants by $\delta\lambda$ and $\delta\mu$, density ρ and its perturbation $\delta\rho$ and strain e_{ij} and its perturbation δe_{ij}. In the frequency domain, we obtain the following equation for the x component:

$$-\rho\omega^2\,\delta u = \partial_x(\lambda\delta\Delta + 2\mu\partial_x\delta u) + 2\partial_y(\mu\delta e_{xy}) + 2\partial_z(\mu\delta e_{zz}) + g_x$$

where

$$g_x = \partial_x(\delta\lambda\Delta + 2\delta\mu\partial_x u) + \partial_y(\delta\mu e_{xy}) + \partial_z(\delta\mu e_{zz}) + \delta\rho\omega^2 u,$$
$$\delta e_{xy} = \tfrac{1}{2}(\partial_y\delta u + \partial_x\delta v),$$
$$\delta e_{xz} = \tfrac{1}{2}(\partial_z\delta u + \partial_x\delta w),$$

and Δ denotes the dilatation of the wavefield. Formulae for other components are obtained by cyclic permutations.

We denote the Green's functions at an angular frequency ω for the reference state by

$$G_{ij}(\mathbf{x}, \mathbf{x}_s; \omega)$$

where j is the direction of a force at the source location $\mathbf{x}_s$ and i is the direction of displacement at the location $\mathbf{x}$. The Green's functions possess the reciprocity relation

$$G_{ij}(\mathbf{x}, \mathbf{x}_s; \omega) = G_{ji}(\mathbf{x}_s, \mathbf{x}; \omega).$$

Using the Green's functions, we can immediately write down the solutions for displacement perturbation; for the x component, we get

$$\delta u = \int_E dv(G_{xx}g_x + G_{xy}g_y + G_{xz}g_z) \tag{3.1}$$

where the arguments for the Green's functions are $(\mathbf{x}_r, \mathbf{x}; \omega)$, where $\mathbf{x}_r$ is the receiver location, and the integral is with respect to $\mathbf{x}$ over the volume of the earth. Expressions for δv and δw can be written down similarly.

By integrating by parts and using the reciprocity relations for the Green's functions, we can obtain the following formula:

$$\delta u = \int_E dv(K_\lambda\delta\lambda + K_\mu\delta\mu + K_\rho\delta\rho) + \int ds\, n_j[\delta\lambda G_{jx}(x, x_r; \omega)\Delta_s + 2\delta\mu G_{ix}(x, x_r; \omega)e_{ij}]^+_-, \tag{3.2}$$

where

$$K_\lambda = -\Delta_r^x\Delta_s,$$
$$K_\mu = -2(E_{xx}^x e_{xx} + E_{yy}^x e_{xx} + E_{zz}^x e_{zz} + 2E_{yz}^x e_{yz} + 2E_{zx}^x e_{zx} + 2E_{xy}^x e_{xy}),$$

and

$$K_\rho = \omega^2(u_r^x u_s + v_r^x v_s + w_r^x w_s).$$

These formulae mean that the kernels, K_λ, K_μ and K_ρ are obtained by multiplying the two wavefields; one generated by the earthquake source and the other by a single force at the source acting in the direction of the component of a seismograph, i.e. the x component in the above example (Fig. 2). Quantities with the superscript x in these formulae correspond to the dilatation (Δ_r^x), displacement and strains (e.g. E_{xx}^x) of the wavefield due to the single force (x component) source at the *receiver* location. Their counterparts, the dilatation Δ_s, displacement and strains (e.g. e_{xx}) are for the wavefields generated by an earthquake source at the *source* location.

The formula (3.2) and its permuted formulae for y and z components can be used for inversion in the 3-D earth. The use of these formulae, however, requires a large memory and much computer time, mainly because of the computation for the kernels. Although there is an algorithm

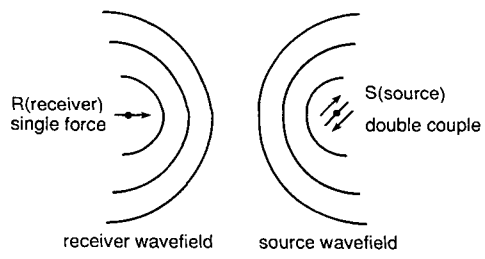

Figure 2. Two wavefields which are needed to compute the kernels in the inverse formulae. The *source* wavefield is due to an earthquake source while the *receiver* wavefield is due to a single force at the receiver. The direction of the single force is the direction of the component (x, y, and z).

developed by Tarantola (1984) which avoids the computation of the kernels, we believe it is important to obtain the kernels in order to understand what is happening during the process of inversion. In the next section, we apply the above formula to surface waves, reducing the problem to 2-D and alleviating the computational problem to a large extent. Also one should note that surface waves usually have the largest amplitudes in the seismograms and direct inversion of seismograms is often dominated by surface wave signals.

3.2 Surface wave formulae

Formulae for surface waves are obtained by simply substituting the surface wave displacement formulae, (2.1) and (2.2), in the above expression (3.2). We first consider the Rayleigh waves. We describe the two wavefields, the earthquake source wavefield and the wavefield due to a single force at the *receiver* by

$$\mathbf{u}_s = U(z)\mathbf{z}\phi_s + V(z)\nabla_1\phi_s$$

and

$$\mathbf{u}_r = U(z)\mathbf{z}\phi_r + V(z)\nabla_1\phi_r$$

respectively. The two potentials, ϕ_s and ϕ_r, have different initial conditions (usually a double couple and a single force), but the formula is valid for any type of source.

Substitution of these formulae in (3.2) yields, after some algebra,

$$\delta u = \int dv[K_1(x, y)\delta\xi_1 + K_2(x, y)\delta\xi_2 + K_3(x, y)\delta\xi_3] + \int ds n_z[K_1(x, y)\delta\eta_1 + K_2(x, y)\delta\eta_2]_-^+$$

where

$$K_1(x, y) = \phi_r\phi_s,$$

$$K_2(x, y) = \frac{\partial^2\phi_r}{\partial x}\frac{\partial\phi_s}{\partial x} + \frac{\partial\phi_r}{\partial y}\frac{\partial\phi_s}{\partial y},$$

$$K_3(x, y) = \frac{\partial^2\phi_r}{\partial x^2}\frac{\partial^2\phi_s}{\partial x^2} + \frac{\partial^2\phi_r}{\partial y^2}\frac{\partial^2\phi_s}{\partial y^2} + 2\frac{\partial^2\phi_r}{\partial x\,\partial y}\frac{\partial^2\phi_s}{\partial x\,\partial y},$$

$$\delta\xi_1 = \delta\rho\omega^2U^2 - \delta\lambda\left(\partial_z U - \frac{\omega^2}{c^2}V\right)^2 - \delta\mu(\partial_z U)^2,$$

$$\delta\xi_2 = \delta\rho\omega^2V^2 - \tfrac{1}{2}\delta\mu(U + \partial_z V)^2$$

$$\delta\xi_3 = -\delta\mu V^2,$$

$$\delta\eta_1 = \delta\lambda U\left(\partial_z U - \frac{\omega^2}{c^2}V\right) + 2\delta\eta U\partial_z U$$

and

$$\delta\eta_2 = \delta\mu V(U + \partial_z V).$$

Here we assumed $|n_x|$, $|n_y| \ll |n_z|$ and dropped terms proportional to n_x and n_y. The notation $[\ ]_-^+$ means the jump across a discontinuity. To avoid clutter, we have dropped the superscript x from ϕ_r. It is understood that the kernels for the perturbation in x displacement (δu) contain the wavefield ϕ_r^x for an x-component force acting at the receiver. Similarly for displacement perturbations δv and δw, we simply substitute ϕ_r^y and ϕ_r^z respectively for ϕ_r.

The case of Love waves can be worked out in a similar way. In this case, we get

$$\delta u = \int dv[K_4(x, y)\delta\xi_4 + K_5(x, y)\delta\xi_5] + \int ds n_z[K_4(x, y)\delta\eta_3]_-^+$$

where K_4 has the same form with K_2 and

$$K_5(x, y) = \frac{1}{2}\left(\frac{\partial^2\phi_r}{\partial x^2} - \frac{\partial^2\phi_r}{\partial y^2}\right)\left(\frac{\partial^2\phi_s}{\partial x^2} - \frac{\partial^2\phi_s}{\partial y^2}\right) + 2\frac{\partial^2\phi_r}{\partial x\,\partial y}\frac{\partial^2\phi_s}{\partial x\,\partial y},$$

$$\delta\xi_4 = \delta\rho\omega^2W^2 - \delta\mu(\partial_z W)^2,$$

$$\delta\xi_5 = -2\delta\mu W^2,$$

and

$$\delta\eta_3 = 2\delta\mu W\partial_z W.$$

3.3 Directional dependence of scattering

Since the potential satisfies

$$\nabla_1^2\phi + \frac{\omega^2}{c^2}\phi = 0$$

it may seem natural to perturb this equation, introducing $\delta\phi$ and δc to this equation, and solving for δc. Such an approach was used, for example, by Yomogida & Aki (1987) recently. However, this approach is not quite correct according to our formulation in the previous section, although the solution cannot be grossly wrong.

The reason for the above statement can been seen by considering a situation given in Fig. 3. In this case, waves due to a single force at the *receiver* location arrive at an angle of Θ from the x axis at point P, while the waves due to the earthquake source arrive at an angle Φ. We take the case of Love waves here. Then by replacing $\partial_x \to ik_x, \ldots$ etc., we obtain

$$K_4 \to -k^2\cos(\Theta - \Phi)\phi_r\phi_s$$

and

$$K_5 \to \tfrac{1}{2}k^4\cos[2(\Theta - \Phi)]\phi_r\phi_s$$

where $k^2 = k_x^2 + k_y^2$. This gives us

$$\delta u = \int dx\,dy\,\phi_r\phi_s\int dz\{k^2(\delta\rho\omega^2W^2 - \delta\mu\partial_z W^2)\cos(\Theta - \Phi) - k^4\delta\mu W^2\cos[2(\Theta - \Phi)]\}.$$

Scattering theory (Sneider 1986; Snieder & Nolet 1987) provides, in essence, the same results. It should be noted,

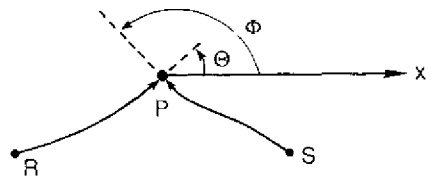

Figure 3. The two wavefields at the point P in a medium. The *source* wavefield makes an angle Φ from the x axis, and the *receiver* wavefield makes an angle Θ.

however, that most theories are derived assuming scatter in a laterally homogeneous medium while the above results are derived for a laterally heterogeneous medium.

If $\Theta - \Phi = \pm\pi$, the z integral in the above equation gives exactly the (negative of) eigenfrequency perturbation, $\delta(\omega^2)$, for Love waves [see for example Takeuchi & Saito (1972); and also the Appendix]. This eigenfrequency perturbation is for a fixed wavenumber k. Then the approximation used by, for example, Yomogida & Aki (1987) which solves δu for δc works, although one must be careful to distinguish $\delta(\omega^2)$ and $\delta(c^2)$, which is measured at fixed frequency in most cases. However because of the terms $\cos(\Theta - \Phi)$ and $\cos[2(\Theta - \Phi)]$, this approach cannot be justified rigorously. Rather, it can be viewed to hold approximately, because it holds along the ray paths. Note that $\Theta - \Phi = \pm\pi$ holds all along the ray paths. Since most contributions to the perturbation come from the region near the ray paths, this approach cannot be grossly in error.

4 IMPORTANCE OF COUPLING BETWEEN DIFFERENT HIGHER MODE BRANCHES

The formulae derived in the previous section can take into account coupling of one branch to another. Coupling of fundamental mode to a higher mode branch, for example, can be evaluated by computing the source wavefield for the fundamental mode branch and the receiver field for a higher mode branch and vice versa. For a complete calculation, one has to extend these calculations for all pairs of relevant higher mode branches. Thus, coupling effects can be taken into account in theory but obviously the method becomes computationally expensive and perhaps not so useful in practice; a complete 3-D calculation will be more efficient at some point, since contributions from various branches will be automatically included. We believe that the attractiveness of the theory applies when one does not have to consider coupling effects.

It is our claim that importance of such couplings can be judged fairly well by examining observed seismograms. Different branches usually possess different group velocities and thus coupling effects produce complicated wavetrains and sometimes new wave packets. In a complicated continental structure, body waves, which are apparently generated by scattering of surface waves, are often observed. Even in an oceanic structure, if the distance is large such as across the Pacific Ocean, short-period surface waves (about 20 s) exhibit long beating waveforms which are most likely due to multipathing effects. Under these circumstances, the coupling effects must be taken into account.

The method can be used to retrieve the large-scale structure of California. In Fig. 4, we show the transverse component seismograms at BKS for the Whittier Narrows earthquake. Four traces are, from top to bottom, the raw Streckeisen (broad-band velocity) records, low-pass filtered records at 50, 75 and 100 mHz. The two numbers at left for the bottom three traces are the frequency range of the cosine taper filter. The second and the third traces show ordinary Love waves. The bottom trace, however, contains two wave packets after the Love waves, which are probably due to reflections from the Sierra Nevada mountains, but we need more data to prove it. Frequency content and their

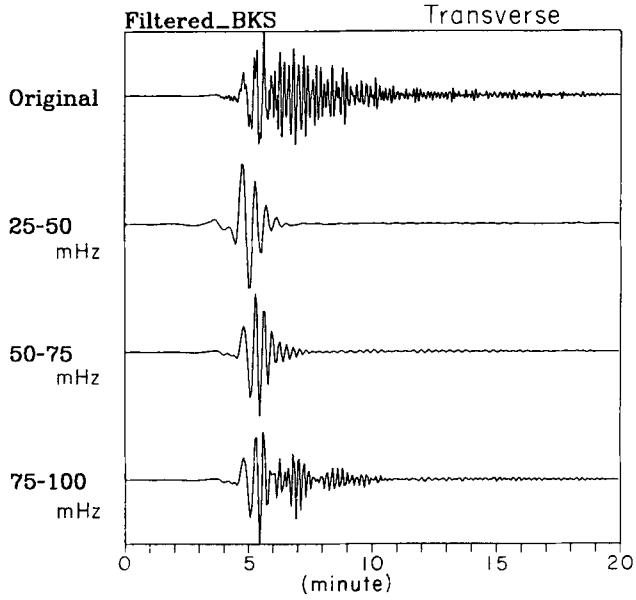

Figure 4. Transverse component seismogram at BKS for the Whittier Narrows earthquake. The raw broad-band (velocity) seismogram is given at top and three low-pass filtered records are given below. The two numbers at left give the frequency range of cosine taper. The second one means, for example, that cosine is one at 25 mHz and goes to zero at 50 mHz. Tick marks at bottom are given at 1 min intervals.

waveforms of these wave packets suggest that they are not fundamental mode waves. In order to model these waves, we will have to consider couplings of fundamental mode branch to higher modes. Fig. 4 also suggests that if we analyse longer period waves, say longer than 20 s, we can avoid coupling calculations.

5 NUMERICAL EXAMPLES

5.1 California

As a first example, we take the case of long-period (10 and 20 s) surface wave propagation in California and show how ray paths are curved in such cases. The power of the method in this paper lies not only in the demonstration of the curved ray paths, since it can also be shown by simple ray tracing calculations, but also in the way the kernels show how different period of waves sample the medium differently.

We have obtained a simple regionalized phase velocity model of California based upon three earthquakes and a Nevada test site explosion. However, in this paper, this model should be viewed as a structure used for forward calculations. Fig. 5 shows our regionalization scheme. This map shows five regions (six regions including the surrounding region) which we assumed to be homogeneous. This regionalization is based on the large-scale geological features at the surface; black regions correspond to crystalline granitic and metamorphic rocks including the Sierra Nevada mountains, the gray region to the central valley (thick unconsolidated sediments), vertical bricks to coastal ranges, vertical bars to Cainozoic volcanoes and horizontal bars to North American cratonic rocks including Mojave desert area. These are certainly rough approximations to the structure and the model is preliminary at the moment.

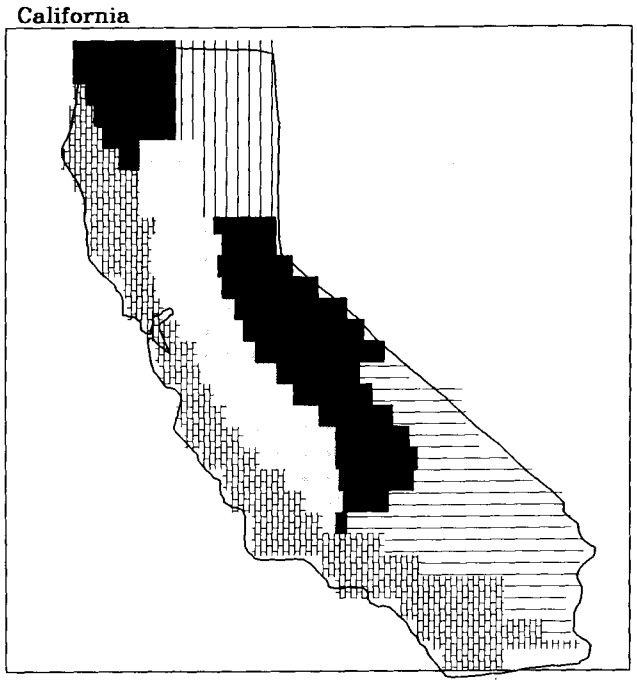

Figure 5. Regionalization scheme for California.

Rayleigh and Love wave phase velocity variations at 20 s are given in Figs 6(a) and (b) respectively, in the top-left figures. Patterns in the two figures correspond to different velocities, however. For Rayleigh waves, dark regions correspond to faster than 3.6 km s^{-1} and the region with horizontal bricks to slower than 3.2 km s^{-1}. Contours are given at every 0.2 km s^{-1}. For Love waves, dark corresponds to faster than 4.0 km s^{-1} while brick patterns correspond to slower than 3.6 km s^{-1} with the same 0.2 km s^{-1} contour interval. Sharp boundaries in Fig. 5 are removed by filtering since the theory cannot handle them as it is presented in the previous section.

We adopted the Cartesian coordinate system and the 2-D wave equation for a potential was solved numerically by the second-order finite difference scheme. The source time function was one cycle of sine function with the period of 20 s. In order to suppress the dispersion due to finite grid size, we introduced small numerical viscosity. Absorbing boundary conditions were applied to minimize artificial reflection from the boundaries (criterion A2 in Clayton & Engquist 1977). The source is assumed to be the Whittier Narrows earthquake but focal mechanism is not taken into account. This is because focusing effects are difficult to understand for a double couple source. We used the phase velocity at 20 s. Effect of dispersion is ignored in this demonstration.

Snap shots of wavefields at times 50, 100, 150, 200 and 250 s are given in both Figs 6(a) and (b). In both Figs 6(a) and (b), wavefronts are similar to cylindrical waves at time 50 s. At 100 s, effects of lateral heterogeneity start to appear. The wavefront near the Sierra Nevada is accelerating while the wavefront near the central valley is slowing down. We also notice amplification in the central valley due to the slow velocity structure in that region. Splitting of wavefronts is visible at 150 s and becomes clearer for figures at 200 and 250 s. At 250 s, we can see the effect of diffraction from the right wavefront, which is laterally refracted from the Sierra Nevada. Since the velocity is faster in the Sierra Nevada than in the central valley, laterally refracted waves arrive earlier than direct waves beyond a certain distance.

We also performed ray tracing calculations for the structures in Figs 6(a) and (b). Results for Rayleigh and Love waves are shown in Figs 7(a) and (b) respectively. Both have very similar patterns. Essentially, as we sweep the rays with the take-off angle from north to northwest, one triplication is encountered. Thus while there are single rays to the two stations in the Sierra Nevada, CMB and ORV, there exist three rays that reach, for example, BKS and WDC. One can imagine various complications in the ray theoretical methods such as asymptotic ray theory or the Gaussian beam method for this type of medium. The proposed method in this paper encounters no problems. For this method, as with many numerical methods, a laterally homogeneous medium is as difficult and time-consuming as a laterally heterogeneous medium.

In Figs 8(a)–(f), we show the shape of kernels, K_1 and K_4 defined in Section 3.2. These kernels give us an intuitive understanding of how surface waves sample the media. In Fig. 8(a), $K_1(x, y)$ for Rayleigh waves at CMB are shown at both 10 and 20 s. Theoretical results for 10 s surface waves are shown here just for comparison with 20 s waves. The structure we used for computation is probably too simple for 10 s waves. The source and receiver locations can be identified by two large amplitude peaks. One can see a fairly broad peak that connects the source and the receiver. Both figures show the curved paths from the source to the receiver. This is of course the effect of high velocity in the Sierra Nevada, along which waves take a detour rather than going straight up through the central valley. This feature is also clear for ORV (Fig. 8b), which shows the Love wave kernels (K_4). The width of the peak is broader for 20 s waves than that for 10 s waves which of course is expected from their wavelength. At the high-frequency limit, the width shrinks down to a very narrow peak, which is essentially the ray path. In the figure, we plotted the ray path between the source and the receiver which was obtained from a separate ray tracing calculation. Ray paths clearly follow the peak of the kernels. One can also visually understand the validity of the stationary phase approximation for short-period waves (10 s) which approximates this peak by a Gaussian curve, ignoring the oscillations outside this peak region.

Figure 8(c) shows the Love wave kernels at SAO. The cases in Figs 8(a)–(c) are simple in that one can clearly trace a peak that connects the source and the receiver; this is because there exists only one ray between the source and the receiver. If there are more than one ray, the kernels and also their interpretations become complicated. Figs 8(d)–(f) show such complicated cases, where there are two rays for MHC and three rays for BKS and WDC. One cannot necessarily trace a peak for each ray any more.

The effects of diffraction can also be found in these kernels. In Fig. 8(a), the kernel at 10 s is simpler than the one at 20 s. Although there is a broad peak for 20 s which corresponds to the ray trajectory, there seem to exist two relatively large peaks west of that broad peak. They

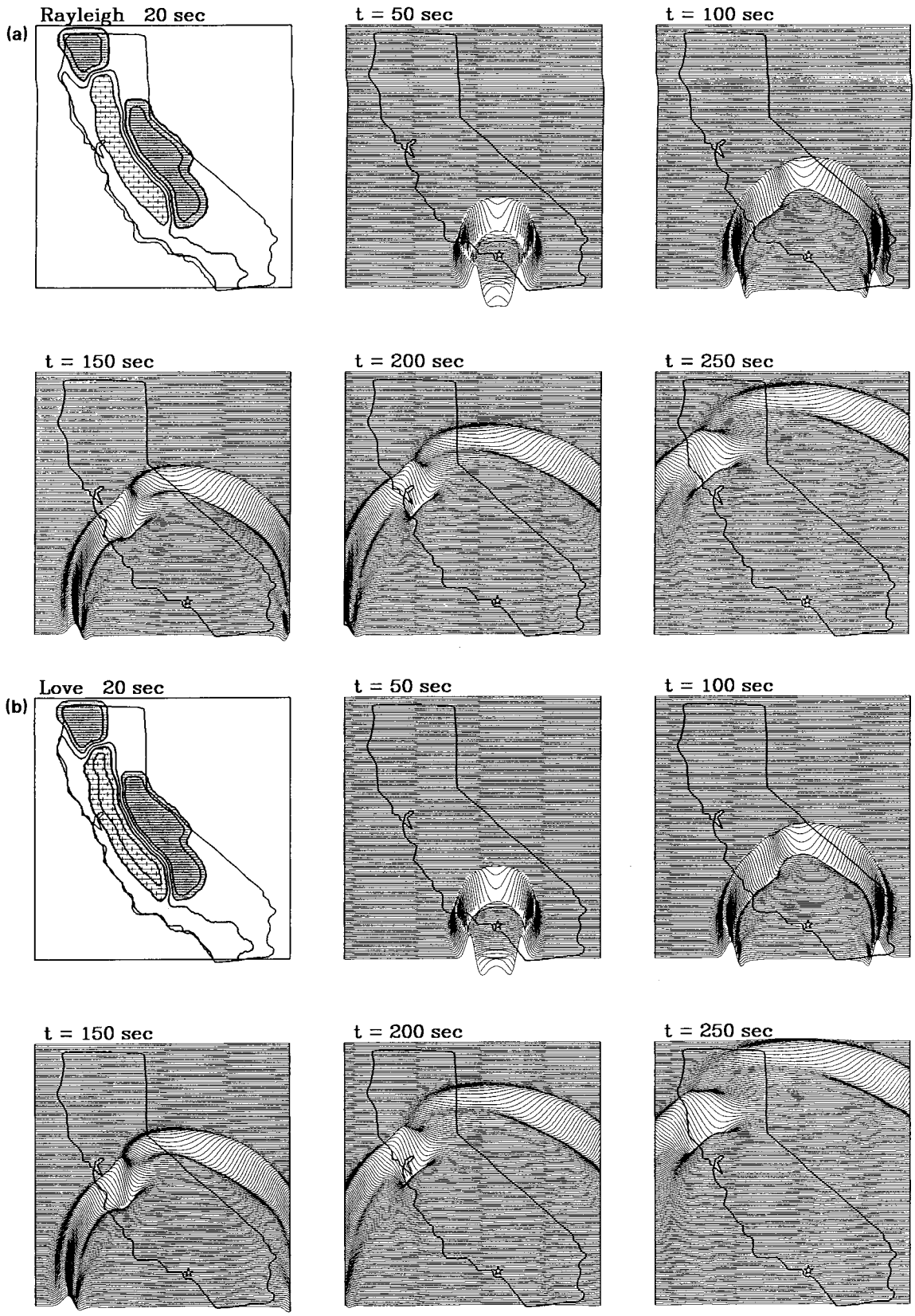

Figure 6. (a) Rayleigh wave phase velocity variation at 20 s is shown in the top-left figure. Dark region is faster than 3.6 km s^{-1}, brick pattern is slower than 3.2 km s^{-1} and contour is at every 0.2 km s^{-1}. Simple simulation for the Whittier Narrows earthquake is shown at times 50, 100, 150, 200 and 250 s after the event. Note that heterogeneity is so severe that the wavefront is split in two by the time it gets to the Bay area. (b) Love wave simulation. Same with Fig. 6(a) except that velocity patterns correspond to different velocity; dark to faster than 4.0 km s^{-1} and brick pattern to slower than 3.6 km s^{-1}.

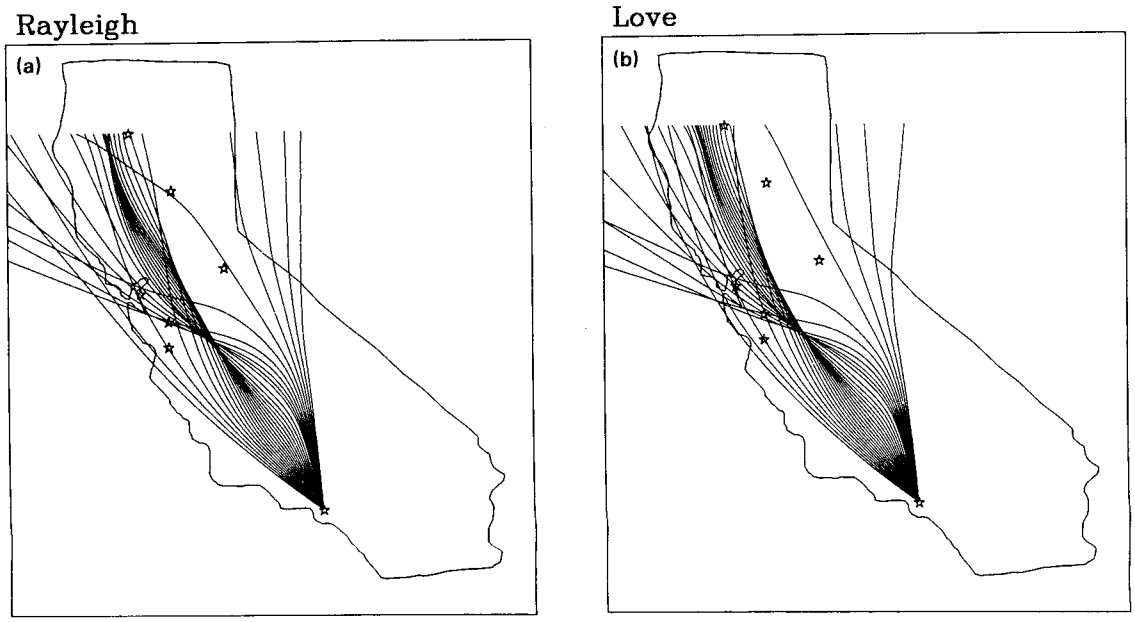

Figure 7. Rays traced for the Rayleigh wave phase velocity model at 20 s. As the rays are swept from north to northwest, one triplication is encountered. (b) Rays traced for the Love wave phase velocity model at 20 s. This is practically the same as Fig. 7(a).

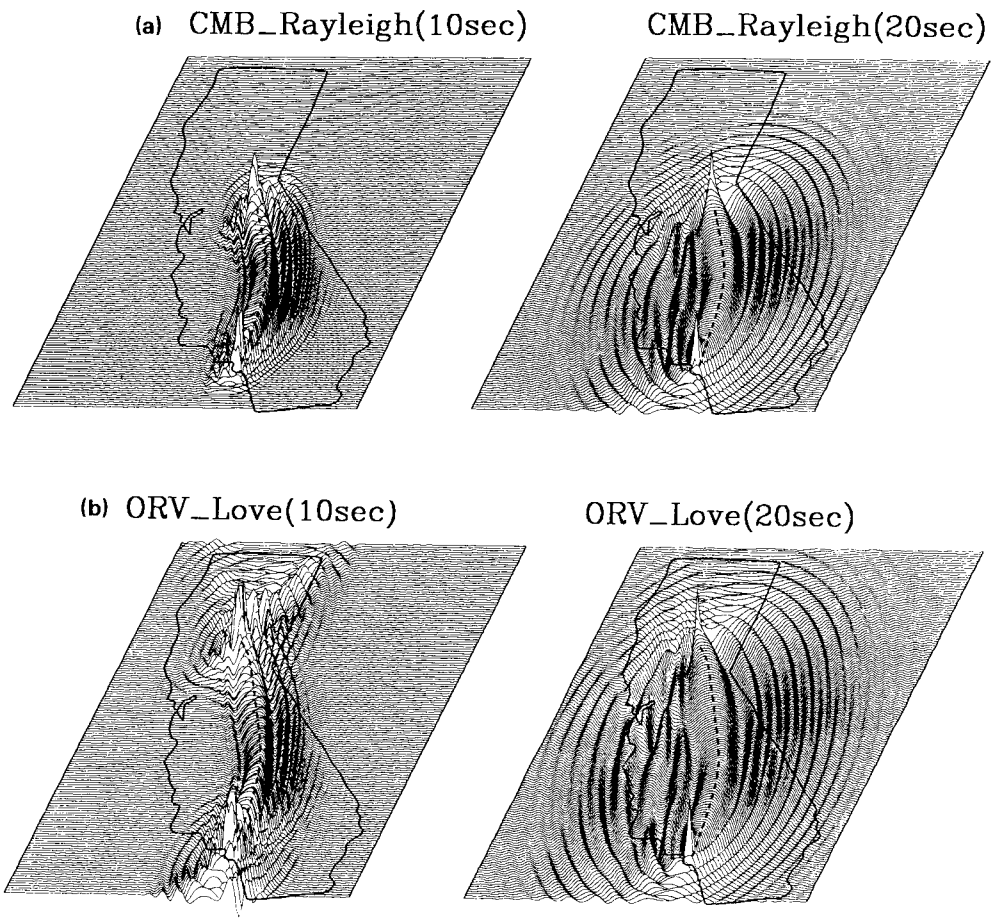

Figure 8. Kernels for the six stations (K_1 and K_4 defined in the Section 3.2). Details are given in the text.

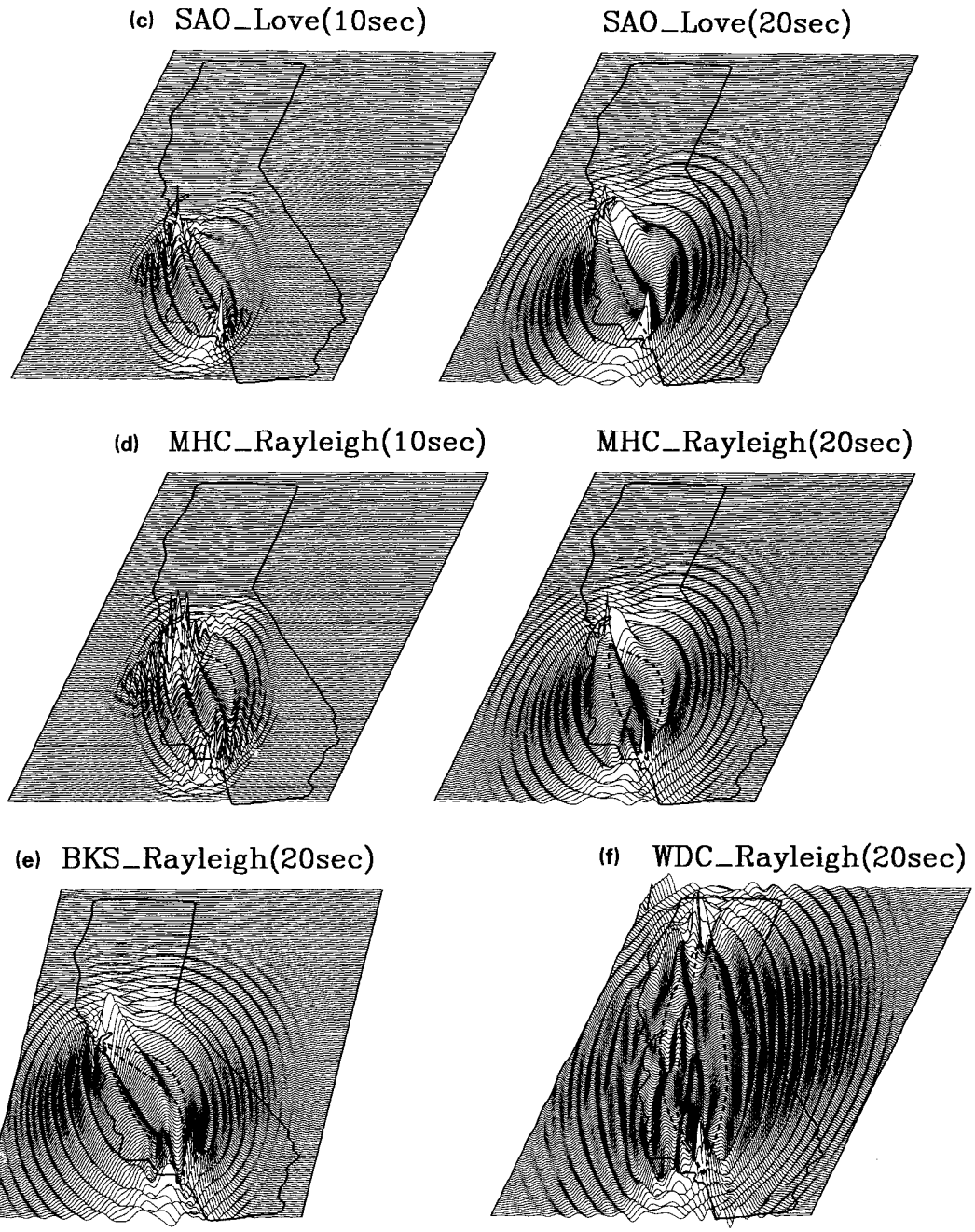

Figure 8. (*continued*)

correspond to energy which is carried by rays that leave the source in the northwest direction and turns northward as they propagate. They do not arrive at CMB, but the cusp of the triplication goes near the station (Fig. 7a). Long-period waves can affect the record at CMB due to the finite wavelength of waves (diffraction effects). Clearly 10 s surface waves have sufficiently short wavelength that secondary peaks do not appear in its kernel.

5.2 Pacific Ocean

The above method is applicable to a larger scale problem, although sphericity must be taken into account in such cases. We developed a computer code to solve the 2-D wave equation on a sphere and applied it to understand the surface wave propagation across the Pacific Ocean.

Our program handles a region on a sphere bounded by lines at constant latitudes and longitudes. Absorbing boundary conditions for the spherical case were developed (Appendix B). They do not suppress the artificial reflections from the boundaries as well as those in the Cartesian coordinates (this is especially true at high latitudes), but reflections can be maintained at reasonably small amplitudes. We used the equal size grid in the following calculations both in latitude and longitude directions. The second-order finite difference scheme is used.

We used the model M84A (Woodhouse & Dziewonski 1984). Phase velocity at each frequency is the input to the

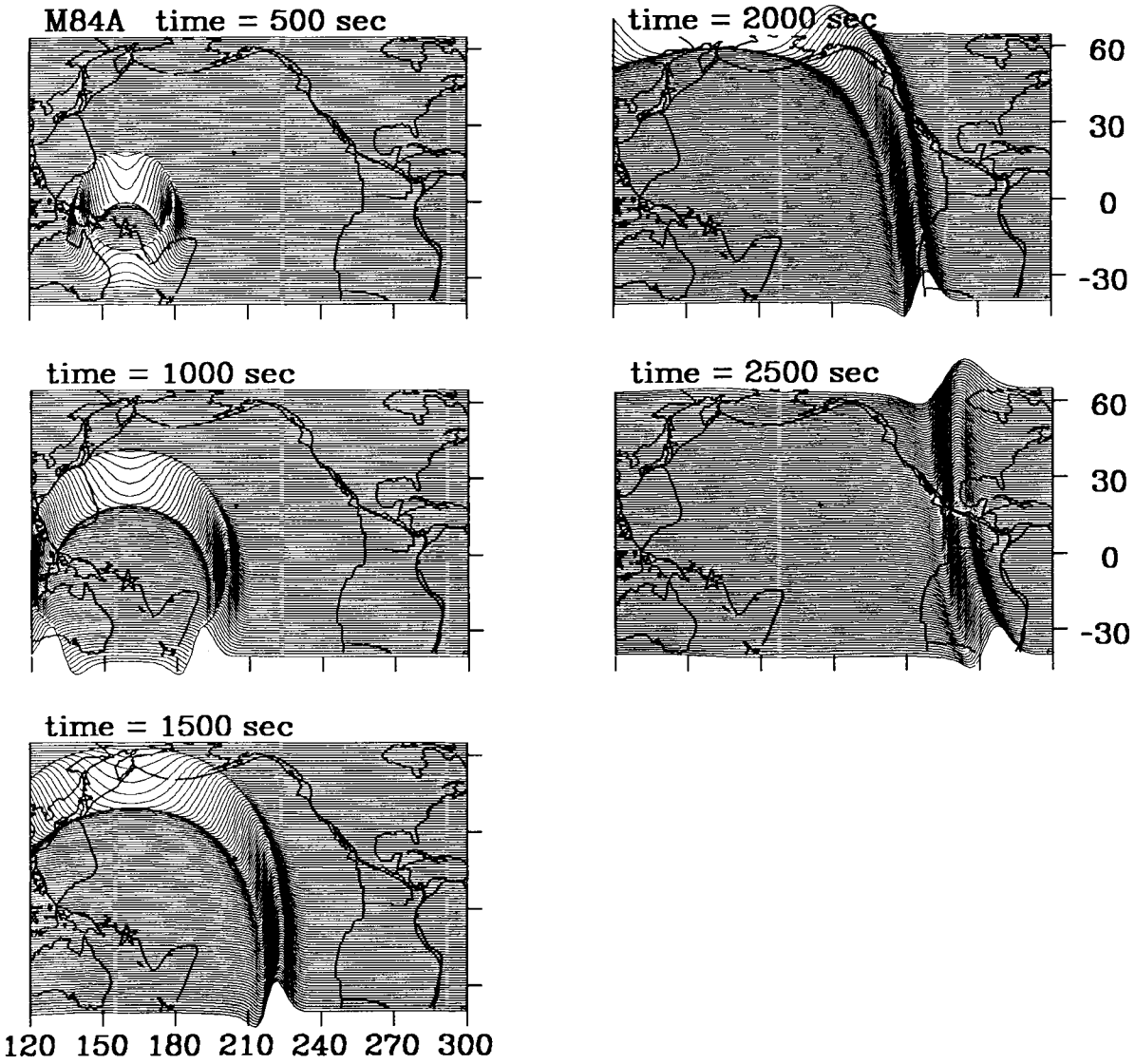

Figure 9. Rayleigh wave simulation on a sphere at the period of 300 s. The model M84A is used for calculation. The results at every 500 s are shown. The degree of heterogeneity is so small that the wavefronts are very smooth.

wave equation. Simulation at 300 s is shown in Fig. 9. The source is located in the Solomon islands and is isotropic (not a double couple). The source time function is one cycle of sine function with period 300 s. Numerical viscosity is again used for the calculations.

Figure 9 shows that heterogeneity in the model is so small that the wavefronts are very smooth. In fact, they are quite similar to those in a homogeneous medium.

Kernels similar to Figs 8(a)–(c) are given in Figs 10(a)–(c). These kernels are computed by multiplication of two wavefields, the source and the receiver wavefields. The receivers are located at Kipapa [KIP, Figs 10(a) and (b)] and Pasadena (Fig. 10c). As expected from the simulation in Fig. 9, these kernels are not different from those in a laterally homogeneous earth. Recent global scale earth models, including M84A, were obtained by assuming that the waves propagate along the great circle paths. This assumption is essentially shown to be internally consistent with the structure obtained in Figs 10(a)–(c). The method in this paper is more useful for shorter period waves (<50 s), when propagation effects become more complicated.

CONCLUSIONS

Surface wave propagation at regional distances show strong effects of lateral refraction even at periods of 10–20 s. In order to analyse these waves, we have developed a new method which takes account of complicated propagation effects such as lateral refraction and multipathing. We also presented the formulae for inversion. Kernels in the inversion formulae give us visual display of how waves sample a medium and are useful in understanding the process of inversion. Taking a preliminary model of California, we demonstrated how ray paths are curved toward six Berkeley stations. The method is attractive in that it can handle complications such as multipathing and the finite wavelength nature of waves automatically. We also demonstrated that the method is applicable to a spherical problem.

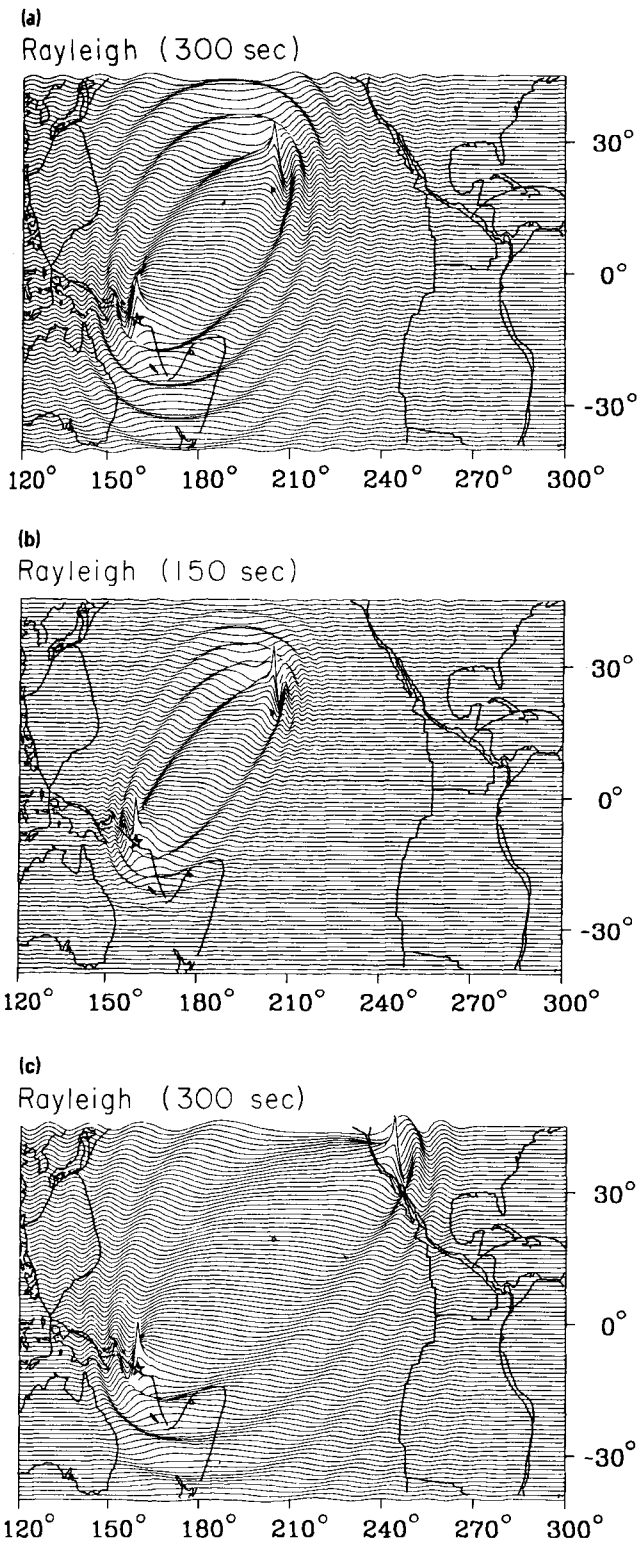

Figure 10. Kernels at Kipapa (a and b) and Pasadena (c) for an assumed source in the Solomon islands. Kernels at 300 s (a and c) and at 150 s (b) are shown. A stationary phase region will emerge as a ray path for short periods (b).

ACKNOWLEDGMENTS

The Berkeley records were kindly supplied by Professor B. A. Bolt and Dr R. Uhrhammer. I had some discussions with Anthony Lomax concerning the effect of the regional geology on wave propagation. This research was supported partially by NSF. Contribution No. 4718, Division of Geological and Planetary Sciences, California Institute of Technology, Padadena, California 91125.

REFERENCES

Bolt, B. A., Lomax, A. & Uhrhammer, R. A., 1989. Analysis of regional broadband recordings of the 1987 Whittier Narrows, California earthquake, *J. geophys. Res.*, **94,** 9557–9568.

Clayton, R. & Engquist, B., 1977. Absorbing boundary conditions for acoustic and elastic wave equations, *Bull. seism. Soc. Am.*, **67,** 1529–1540.

Dahlen, F. A., 1980. A uniformly valid asymptotic representation of normal mode multiplet spectra on a laterally heterogeneous Earth, *Geophys. J. R. astr. Soc.*, **62,** 225–247.

Dahlen, F. A. & Henson, I. H., 1985. Asymptotic normal modes of a laterally heterogeneous Earth, *J. geophys. Res.*, **90,** 12 653–12 681.

Hadley, D. & Kanamori, H., 1977. Seismic structure of the transverse ranges, *Geol. Soc. Am. Bull.*, **88,** 1469–1478.

Henson, I. H. & Dahlen, F. A., 1986. Asymptotic normal modes of a laterally heterogeneous Earth 2. Further results, *J. geophys. Res.*, **91,** 12 467–12 481.

Park, J., 1987. Asymptotic coupled-mode expressions for multiplet amplitude anomalies and frequency shifts on an aspherical earth, *Geophys. J. R. astr. Soc.*, **90,** 129–169.

Snieder, R., 1986. 3-D linearized scattering of surface waves and a formalism for surface wave holography, *Geophys. J. R. astr. Soc.*, **84,** 581–605.

Snieder, R. & Nolet, G., 1987. Linearized scattering of surface waves on a spherical Earth, *J. Geophys.*, **611,** 55–63, 1987.

Sword, C. H., Claerbout, J. F. & Sleep, N. H., 1989. Modelling of global surface waves by a finite element method, *Geophys. J. R. astr. Soc.*, submitted.

Takeuchi, H. & Saito, M., 1972. Seismic surface waves, *Meth. Comp. Phys.*, **11,** 217–295.

Tanimoto, T., 1988. The 3-D shear wave structure in the mantle by overtone waveform inversion II. Inversion of X-waves, R-waves and G-waves, *Geophys. J. R. astr. Soc.*, **93,** 321–334.

Tarantola, A., 1984. Inversion of seismic reflection data in the acoustic approximation, *Geophysics*, **49,** 1259–1266.

Tsuboi, S. & Geller, R., 1989. Coupling between the multiplets of laterally heterogeneous earth models, *Geophys. Res. Lett.*, **96,** 371–379.

Woodhouse, J. H. & Dziewonski, A. M., 1984. Mapping the upper mantle: Three-dimensional modeling of earth structure by inversion of seismic waveforms, *J. geophys. Res.*, **89,** 5953–5986.

Woodhouse, J. H. & Wong, Y. K., 1986. Amplitude, phase and path anomalies of mantle waves, *Geophys. J. R. astr. Soc.*, **87,** 753–773.

Yomogida, K., 1985. Gaussian beams for surface waves in laterally slowly varying media, *Geophys. J. R. astr. Soc.*, **82,** 511–533.

Yomogida, K. & Aki, K., 1987. Amplitude and phase data inversions for phase velocity anomalies in the Pacific Ocean basin, *Geophys. J. R. astr. Soc.*, **88,** 161–204.

APPENDIX A

In this appendix, we show that the validity of the formulae (2.1)–(2.3). We substitute (2.1) and (2.2) into the elastodynamic equations of motion and show that the potential must satisfy (2.3). We assume that lateral variations of elastic constants are smooth and approximations such as (2.4) are valid.

We consider the case of Rayleigh waves first. By substituting (2.1) into the equations of motion in the frequency domain, we obtain the following formulae for the x, y and z components respectively:

$$-\rho\omega^2 V\frac{\partial\phi}{\partial x}=(\lambda+2\mu)v\frac{\partial^3\phi}{\partial x^3}+\lambda V\frac{\partial^3\phi}{\partial x\,\partial y^2}+\lambda\partial_z U\frac{\partial\phi}{\partial x}+2\mu V\frac{\partial^2\phi}{\partial x\,\partial y^2}+\partial_z[\mu(U+\partial_z V)]\frac{\partial\phi}{\partial x}, \quad \text{(A1)}$$

$$-\rho\omega^2 V\frac{\partial\phi}{\partial y}=2\mu V\frac{\partial^3\phi}{\partial x^2\,\partial y}+\lambda V\frac{\partial^3\phi}{\partial x^2\,\partial y}+(\lambda+\mu)V\frac{\partial^3\phi}{\partial y^3}+\lambda\partial_z U\frac{\partial\phi}{\partial y}+\partial_z[\mu(U+\partial_z V)]\frac{\partial\phi}{\partial y}, \quad \text{(A2)}$$

$$-\rho\omega^2 U\phi=\mu(U+\partial_z V)\frac{\partial^2\phi}{\partial x^2}+\mu(U+\partial_z V)\frac{\partial^2\phi}{\partial y^2}+\partial_z(\lambda V)\nabla_1^2\phi+\partial_z[(\lambda+2\mu)\partial_z U]\phi. \quad \text{(A3)}$$

If we transform from (x, y) to (k_x, k_y) by the Fourier transformation, we can always write

$$\nabla_1^2\phi+k^2\phi=0, \quad \text{(A4)}$$

where $k_x^2+k_y^2=k^2$, although k is not necessarily the wavenumber for the Rayleigh waves. At this point we do not know whether this k is related to ω/c, where c is the local phase velocity. The fact that it is so can be verified by multiplying $V(\partial\phi^*/\partial x)$ to (A1), $V(\partial^*/\partial y)$ to (A2) and $U\phi^*$ to (A3), adding all of them and integrating with respect to the z coordinate; we obtain

$$\omega^2 I_1=I_2 \quad \text{(A5)}$$

where

$$I_1=\int dz\,\rho(U^2+k^2V^2), \quad \text{(A6)}$$

$$I_2=\int dz\{\lambda(\partial_z U-k^2V)^2+\mu[2(\partial_z U)^2+2k^4V^2+(U+\partial_z V)^2k^2]\}. \quad \text{(A7)}$$

If we replace $kV\rightarrow V$, this is exactly the variational relationship that Rayleigh waves satisfy for the structure given by $\rho(z)$, $\lambda(z)$ and $\mu(z)$ (e.g. Takeuchi & Saito 1972, p. 262). This means that the wavenumber k is truly the horizontal wavenumber for the surface waves and one can write $k=\omega/c$, where c is the local phase velocity for Rayleigh waves. Note that since the variational principle holds up the first-order perturbation in eigenfunctions, the assumption of keeping U and V constant as the waves propagate is valid to first order.

In the case of Love waves, similar derivation yields

$$I_1=\int\rho k^2W^2\,dz$$

and

$$I_2=\int dz k^2[\mu(\partial_z W)^2+k^2\mu W^2]$$

which is the variational principle for Love waves, if we substitute $kW\rightarrow W$. The same argument holds in this case and the potential, ϕ_T, satisfies

$$\nabla_1^2\phi_T+\frac{\omega^2}{c(x,y)^2}\phi_T=0$$

where c is the local Love wave phase velocity.

APPENDIX B: ABSORBING BOUNDARY CONDITIONS ON A SPHERE

We will employ asymptotic formulae in the following derivation. Thus the formulae will naturally have problems at high latitudes. According to our experience, they work fairly well up to about 75 degrees.

If we employ the asymptotic approximation such as $\partial_\theta\phi\approx\pm i[(l+1/2)\phi]$, the dispersion relation for the 2-D wave equation on a sphere becomes

$$\frac{\omega^2r^2}{c^2}\approx\left(l+\frac{1}{2}\right)^2+\frac{m^2}{\sin^2\theta} \quad \text{(B1)}$$

where l is the angular degree and m is the azimuthal order, and r is the radius of the Earth. Following Clayton & Engquist (1977), we obtain the outgoing wave conditions at each boundary and translate the equations back to partial differential equations. We then obtain the following formulae:

$$\frac{1}{\sin\theta}\partial_t\partial_\phi\phi+\frac{r}{c}\partial_t^2\phi-\frac{c}{2r}\partial_\phi^2\phi=0, \quad \text{(east)},$$

$$\frac{1}{\sin\theta}\partial_t\partial_\phi\phi-\frac{r}{c}\partial_t^2\phi+\frac{c}{2r}\partial_\theta^2\phi=0, \quad \text{(west)},$$

$$\partial_t\partial_\theta\phi-\frac{r}{c}\partial_t^2\phi+\frac{c}{2r\sin^2\theta}\partial_\phi^2\phi=0, \quad \text{(north)},$$

$$\partial_t\partial_\theta\phi+\frac{r}{c}\partial_t^2\phi-\frac{c}{2r\sin^2\theta}\partial_\phi^2\phi=0, \quad \text{(south)}.$$

Discretized froms for these formulae are used in the computations for the spherical cases.